A&A 603, A24 (2017)
DOI: 10.1051/0004-6361/201730538

Astronomy & Astrophysics

Optical spectroscopy of the Be/X-ray binary V850 Centauri/GX 304-1 during faint X-ray periodical activity

C. Malacaria[1], W. Kollatschny[2], E. Whelan[3], A. Santangelo[1,4], D. Klochkov[1], V. McBride[5,6], and L. Ducci[1,7]

[1] Institut für Astronomie und Astrophysik, Sand 1, 72076 Tübingen, Germany
e-mail: malacaria@astro.uni-tuebingen.de
[2] Institut für Astrophysik, Universität Göttingen, Friedrich-Hund Platz 1, 37077 Göttingen, Germany
[3] Maynooth University Department of Experimental Physics, National University of Ireland Maynooth, Maynooth Co. Kildare, Ireland
[4] Institute of High Energy Physics, Chinese Academy of Sciences, 100049 Beijing, PR China
[5] Department of Astronomy, University of Cape Town, Private Bag X3, 7701 Rondebosch, South Africa
[6] South African Astronomical Observatory, PO Box 9, Observatory, 7935 Cape Town, South Africa
[7] ISDC Data Center for Astrophysics, Université de Genève, 16 chemin d'Écogia, 1290 Versoix, Switzerland

Received 31 January 2017 / Accepted 25 April 2017

ABSTRACT

Context. Be/X-ray binaries (BeXRBs) are the most populous class of high-mass X-ray binaries. Their X-ray duty cycle is tightly related to the optical companion wind activity, which in turn can be studied through dedicated optical spectroscopic observations.
Aims. We study optical spectral features of the Be circumstellar disk to test their long-term variability and their relation with the X-ray activity. Special attention has been given to the Hα emission line, one of the best tracers of the disk conditions.
Methods. We obtained optical broadband medium resolution spectra from a dedicated campaign with the Anglo-Australian Telescope and the Southern African Large Telescope in 2014−2015. Data span over one entire binary orbit, and cover both X-ray quiescent and moderately active periods. We used Balmer emission lines to follow the evolution of the circumstellar disk.
Results. We observe prominent spectral features, like double-peaked Hα and Hβ emission lines. The Hα V/R ratio significantly changes over a timescale of about one year. Our observations are consistent with a system observed at a large inclination angle ($i \gtrsim 60°$). The derived circumstellar disk size shows that the disk evolves from a configuration that prevents accretion onto the neutron star, to one that allows only moderate accretion. This is in agreement with the contemporary observed X-ray activity. Our results are interpreted within the context of inefficient tidal truncation of the circumstellar disk, as expected for this source's binary configuration. We derived the Hβ-emitting region size, which is equal to about half of the corresponding Hα-emitting disk, and constrain the luminosity class of V850 Cen as III–V, consistent with the previously proposed class.

Key words. stars: individual: V850 Cen – stars: individual: GX 304-1 – stars: emission-line, Be – stars: neutron – X-rays: binaries

1. Introduction

V850 Cen/GX 304-1 is a Be/X-ray binary (BeXRB) system composed of a B2 Vne optical companion (V850 Cen, $m_R \sim 12.6$) and a pulsating neutron star (NS, McClintock et al. 1977), located at a distance of 2.4 ± 0.5 kpc (Parkes et al. 1980). The first X-ray emission from this system was detected in 1967 during a balloon observation (Hewish et al. 1968; Lewin et al. 1968), while the optical counterpart was discovered only ten years later, using data from the Anglo-Australian Telescope (AAT) by Mason et al. (1978).

BeXRBs are characterized by luminous X-ray outbursts powered by the accretion of matter onto the NS. The accreted matter is supplied by the Be star, whose stellar wind is expelled under the form of a circumstellar equatorial disk, which can be extended up to many stellar radii (Rivinius et al. 2013). Typically, X-ray (Type I) outbursts in BeXRBs take place at each periastron passage, where the disk is closer to the NS orbit and the gravitational influence of the NS is stronger. They are therefore characterized by a periodical recurrence identical to the orbital period.

The circumstellar decretion disk is a geometrically thin, high-density plasma rotating at a nearly Keplerian speed, and is observationally determined by infrared (IR) excess and by Balmer emission lines in the optical band, especially the Hα emission line (Porter & Rivinius 2003). In fact, spectral parameters of the Hα line (such as the equivalent width (EW), the full width at half maximum (FWHM), and others) provide quantitative information on the circumstellar disk structure, its size and density distribution (see e.g. Grundstrom & Gies 2006, and references therein).

In certain cases, circumstellar disks in BeXRBs are truncated by the gravitational influence of the NS (Negueruela & Okazaki 2001; Monageng et al. 2017, and references therein), thus becoming optically thick at IR wavelengths and subject to radiation-driven instabilities. Under the influence of such instabilities, the disk becomes warped, tilted, and precessing (Porter 1998). Once deformed, the circumstellar disk can transfer matter onto the NS at different orbital phases than the periastron, thus powering giant (Type II) outbursts or shutting down the periodical ones (Okazaki et al. 2013; Martin et al. 2014, and references therein). Therefore, the X-ray activity and the Be-disk status are tightly entwined and need to be studied together.

The X-ray history of GX 304-1 is studded with both active and quiescent periods. After its first X-ray detection, the

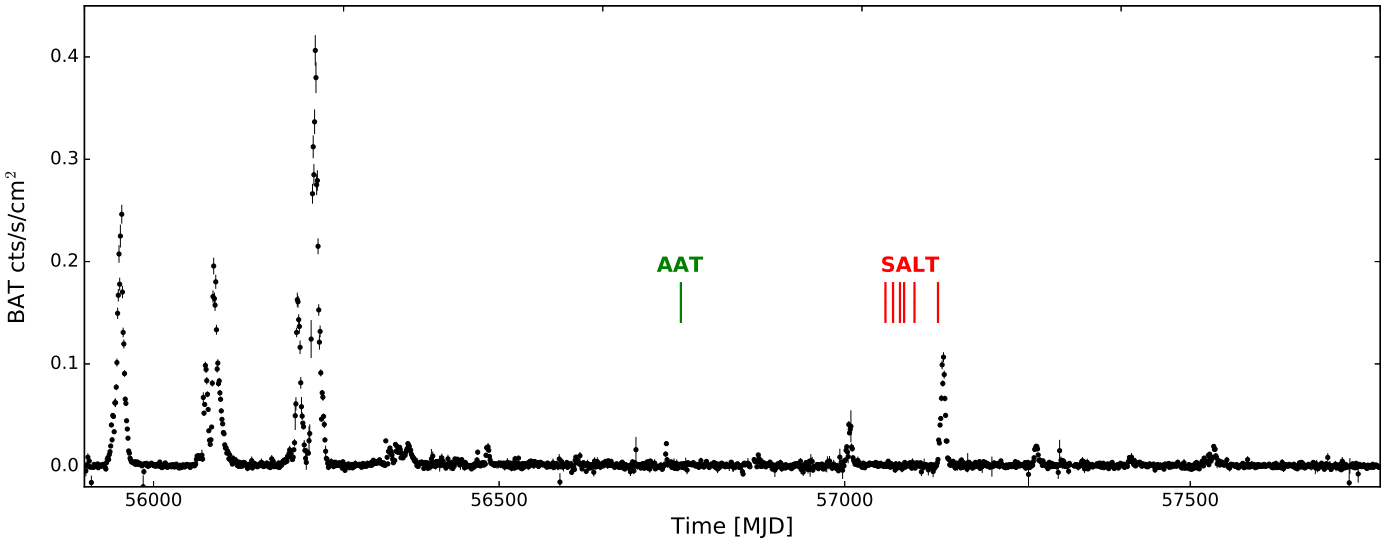

Fig. 1. *Swift*/BAT [15−50 keV] light curve of the long term GX 304-1 X-ray activity. Superimposed are the AAT/UCLES (2014 − green bar) and SALT/HRS (2015 − red bars) observations.

Table 1. Journal of V850 Cen optical observations with AAT/UCLES and SALT/HRS.

Program & block ID	Seeing (arcsec)	Date & pointing time	Exposure [ks]	Filter
AAT UCLES + EEV2 UC205	1.50	2014-04-16 12:35 [UT]	2×1200	–
2014-2-SCI-077 P1 HRS 32843	1.36	2015-02-06 01:23 [SAST]	940	SDSSr-S
2014-2-SCI-077 P1 HRS 32840	1.20	2015-02-17 01:32 [SAST]	940	SDSSi-S1
2014-2-SCI-077 P2 HRS 32841	1.90	2015-02-27 01:04 [SAST]	1034	SDSSg-S1
2014-2-SCI-077 P2 HRS 32842	1.60	2015-03-05 23:20 [SAST]	1034	SDSSi-S
2014-2-SCI-077 P3 HRS 32844	1.36	2015-03-20 03:02 [SAST]	940	SDSSr-S1
2014-2-SCI-077 P2 HRS 32839	1.54	2015-04-23 21:42 [SAST]	1034	SDSSi-S1

source was regularly outbursting with a ∼132.5 d periodicity (Priedhorsky & Terrell 1983), which was interpreted as the orbital period. The periodical X-ray activity lasted until around 1984 (Pietsch et al. 1986), when the source entered a long period with no detectable X-ray emission, that is, a quiescent phase. The source resumed its activity only 28 yr later, in June 2008, when it was detected in the hard X-ray band by INTEGRAL (Manousakis et al. 2008). Since then, GX 304-1 resumed its periodical outburst activity, with typical peak luminosities of 10^{36-37} erg/s. The new active period lasted for ∼6 yr, and its last outburst was a giant one, characterized by an X-ray luminosity of $\sim 2 \times 10^{37}$ erg/s and a double-peaked light curve whose peaks were centered far from the periastron. Afterwards, the source turned into another quiescent period, showing only sporadic weak outbursts at periastron passages (see, e.g., Nakajima et al. 2015).

Despite GX 304-1 being a luminous X-ray transient that has furnished a wealth of information on the physics of accreting pulsars (Devasia et al. 2011; Yamamoto et al. 2011; Klochkov et al. 2012; Malacaria et al. 2015; Jaisawal et al. 2016; Rothschild et al. 2017), optical studies of V850 Cen are rare. However, early observations of V850 Cen during the 28 yr X-ray quiescent period showed that the optical spectrum initially exhibited strong double-peaked Hα line that progressively faded out, eventually leaving only the absorption feature (Corbet et al. 1986; Haefner 1988). The lack of Hα line from V850 Cen reflects the depletion of the Be-disk, which turned off the X-ray source (Pietsch et al. 1986).

Here we present a spectroscopic study of V850 Cen in the wavelength range 4500 to 8900 Å. Observations were obtained between April 2014 and April 2015, when the X-ray source was showing only moderate activity. The results presented here are focused on a spectral analysis of the Hα line, with the aim of probing the Be circumstellar decretion disk, and thus the connection between the disk and the X-ray activity of the NS.

2. Observations and data reduction

Optical spectroscopic observations of V850 Cen were performed with two ground-based telescopes: the 3.9 m Anglo Australian Telescope (AAT) and the 10 m Southern African Large Telescope (SALT). A log of the observations is given in Table 1, while Fig. 1 shows the optical observations superimposed to the X-ray long-term light curve of GX 304-1.

The first observation was obtained on 2014, April 16th, at the AAT with the University College London Echelle Spectrograph (UCLES, Horton et al. 2012). UCLES is a high-resolution spectrograph ($R > 40\,000$) sensitive in the range 4500−8900 Å. The source was observed with a 2×20 min exposure and a 1.″5 slit width while the seeing was 1.″50. Both runs were carried out with the 31 line/mm cross-dispersing grating and the EEV2 CCD

Table 2. Spectral parameters of the Hα emission line and derived disk radii.

MJD (ϕ_{orb})	EW	$FWHM$	ΔV	V/R	$V \sin i$ [km s^{-1}]				R_{disk}
	[Å]	[Å] (km s^{-1})	[km s^{-1}]		Eq. (1)	Eq. (2a)	Eq. (2b)	Eq. (3)	[$R_\star$]
56 763 (0.12)	-14.1 ± 0.7	7.8 ± 0.1 (367 ± 3)	252 ± 3	0.22 ± 0.03	226	466	323	218	5.9 ± 0.3
57 059 (0.36)	-36.4 ± 1.2	7.4 ± 0.1 (342 ± 3)	185 ± 6	0.83 ± 0.02	209	463	325	223	11.1 ± 3.5
57 070 (0.44)	-32.3 ± 0.9	7.1 ± 0.1 (326 ± 3)	180 ± 3	0.75 ± 0.01	197	434	304	210	10.2 ± 1.8
57 080 (0.52)	-33.0 ± 1.2	7.3 ± 0.2 (337 ± 4)	189 ± 3	0.73 ± 0.02	205	458	321	218	10.4 ± 2.1
57 086 (0.56)	-39.0 ± 1.3	7.3 ± 0.2 (334 ± 3)	191 ± 3	0.73 ± 0.03	203	489	343	220	11.6 ± 2.8
57 101 (0.68)	-32.8 ± 1.5	7.6 ± 0.2 (354 ± 4)	200 ± 3	0.84 ± 0.01	217	484	339	229	10.3 ± 2.3
57 135 (0.94)	-27.0 ± 1.3	8.1 ± 0.4 (366 ± 4)	224 ± 9	0.75 ± 0.05	226	507	356	232	9.1 ± 2.1

(with a central wavelength of 5450 Å). The chip was read out in "normal" mode, with a readout noise of 3.9 electrons.

The second set of observations was carried out at the SALT with the High Resolution Spectrograph (HRS, Tyas 2012). SALT/HRS is a dual-beam (blue arm 370−555 nm and red arm 555−890 nm) fibre-fed echelle spectrograph, with a single $2k \times 4k$ CCD to capture all the blue orders, while a $4k \times 4k$ detector is used for the red orders. HRS was always set up in the Medium Resolution Mode ($R \sim 40\,000$), whose readout speed is 400 kHz for both arms and the slit width is 0.″7. The CCDs binning was the standard 1×1 in the spatial direction, that is optimized for the spectral resolution. Due to problems with the CCD in the blue arm science frame (blue spectra suffer from instrumental contamination and are complicated by multiple readout amplifiers), here we have only used SALT red arm data.

All data have been reduced using standard IRAF[1] packages (version 2.16), and all images have been both bias- and flatfield-corrected. Wavelength calibration has been applied using arc (thorium−argon) lamp spectra. Flux calibration was not applied, since the spectra were used to measure spectral parameters of emission features and to locate the peaks of the double-peaked emission lines.

3. Results

3.1. The rotational velocity

It is known that Be stars are rapid rotators, and their rotational velocity can be measured using emission or absorption line parameters. Steele et al. (1999) provide the relations between the projected rotational velocity $V \sin i$ (where i is the inclination angle under which the observer sees the disk plane) and the FWHM of He I lines. Those relations have been largely employed in the literature (see, e.g. Rajoelimanana et al. 2017; Reig et al. 2010, 2004; Kızıloğlu et al. 2007). However, He I lines lie in the blue part of the stellar spectrum, which is not available in our case (see Sect. 2). On the other hand, Hanuschik (1989) derived the relations between $V \sin i$ and the spectral parameters of the Hα emission line, that is, the peak separation ΔV (in case of double-peaked lines), the EW, and the FWHM. Those relations are described in the following equations, where the $V \sin i$ is given as a function of the FWHM:

$$FWHM(H\alpha) = 1.4 V \sin i + 50 \,\mathrm{km\,s^{-1}}, \quad (1)$$

as a function of ΔV and EW:

$$\log\left(\frac{\Delta V}{2V \sin i}\right) = -0.32 \log EW(H\alpha) - 0.20, \quad (2a)$$

[1] Image Reduction and Analysis Facility: `iraf.noao.edu`

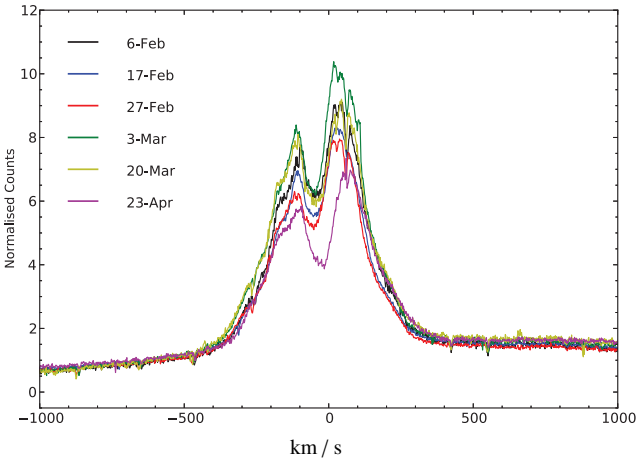

Fig. 2. Evolution of the Hα emission line profile, as observed by SALT/HRS during one entire orbital period at the beginning of 2015.

or as a function of FWHM and EW:

$$\log\left(\frac{FWHM}{2V \sin i}\right) = -0.1 \log EW(H\alpha) + 0.04, \quad (3)$$

with ΔV, FWHM, and $V \sin i$ measured in km s^{-1}, while EW in Å (where the absolute value of EW is considered as the argument of the logarithm).

Because the fit parameters are reported without errors in Hanuschik (1989), a realistic error calculation on the derived $V \sin i$ values is not possible. Following van Belle (2008) for an estimation of the error on $V \sin i$ we considered the range shown by the data points in Figs. 1, 4, and 8 in Hanuschik (1989), from which Eqs. (1), (3), and (2a), respectively, have been obtained. The resulting errors on $V \sin i$ are 50, 40, and 110 km s^{-1} for Eqs. (1), (3), and (2a), respectively.

We calculated EWs for double-peaked profiles by direct integration of the flux across the feature using the *splot* task of IRAF. The same task has been used to obtain FWHMs by fitting a single Gaussian profile over the entire double-peaked feature, which fits well the overall line shape. Furthermore, the double-peaked profiles have also been fitted using the deblending routine available in IRAF. The two peaks have been modeled with two Voigt functions, which fitted the line wings better than Gaussian functions. This allowed us to obtain line centers and intensity of the two peaks above the continuum. These, in turn, allowed us to calculate the so-called V/R ratio, defined as the relative intensity of the blue (V) and red (R) peaks in the split profile of the line, and the peak separation ΔV. Following the methodology of Reig et al. (2010), to derive all Hα lines spectral parameters the

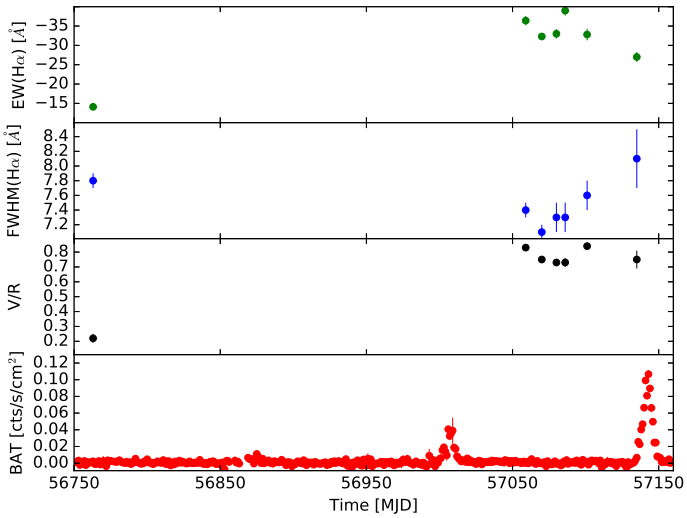

Fig. 3. Variability of the Hα line spectral parameters compared to the X-ray flux as a function of time. Panels show, *from top to bottom*, the Equivalent Width (EW), the Full Width Half Maximum (FWHM), the V/R ratio, and the *Swift*/BAT X-ray count rate, while on the x-axis is reported the time in MJD.

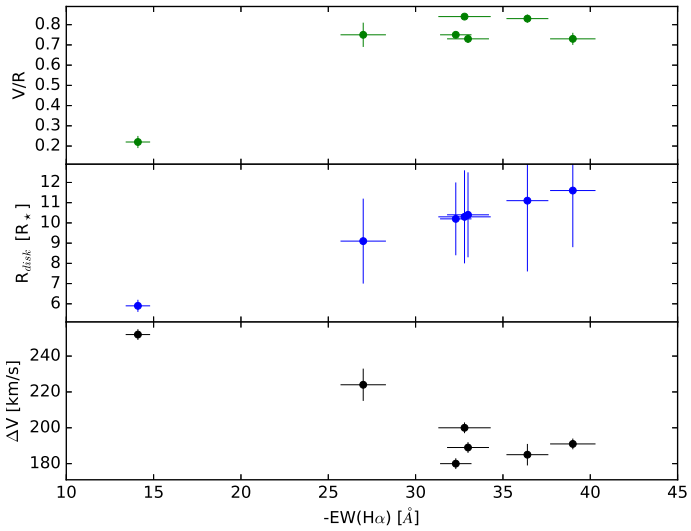

Fig. 4. Correlations between the Hα line-related parameters and the Hα Equivalent Width. Panels show on the y-axis, from top to bottom, the V/R ratio, the circumstellar disk radius calculated from Eq. (8), and the peak separation ΔV, while on the x-axis is reported the EW absolute value.

fitting procedure has been iterated twelve times for each double-peaked feature. Since the main source of uncertainty in the EW is due to the difficult definition of the continuum, at each iteration a slightly different point of the continuum was sampled. Final values and errors of line parameters have been calculated as the average and standard deviation over those iterated measures.

The results are given in Table 2. Values of $V \sin i$ obtained by Eqs. (1), (2a), (3) show different nominal values (consistent within the large errors). However, it is important to note that those relations are obtained for isolated Be stars, while circumstellar disks of BeXRBs are about 1.5−2 times denser than those of isolated Be stars (Zamanov et al. 2001; Reig et al. 2016). Such an effect has been attributed to disk truncation, although those works find higher disk densities also for BeXRBs with long orbital periods, in which disk truncation is expected to be inefficient (see Sect. 3.4). Hanuschik et al. (1988) relates the disk density to the intercept of Eq. (2a) (see Eq. (8) of their work), while Monageng et al. (2017) find that for a group of BeXRBs, the best-fit solution of $\log(\frac{\Delta V}{2V \sin i})$ versus $\log(\frac{-EW}{\text{Å}})$ results in the new relation:

$$\log\left(\frac{\Delta V}{2V \sin i}\right) = -0.33 \log EW(\text{H}\alpha) - 0.03. \quad (2b)$$

Equation (2b) returns an average projected velocity of $\sim 330 \pm 55\,\text{km s}^{-1}$. Since this value has been obtained using a relationship that is calibrated on BeXRBs, we use this as a reference value in the following.

Be stars are believed to rotate at ∼60−80% of their critical velocity (Porter 1996; Rivinius et al. 2006). Earlier observations of the V850 Cen Hα line (Parkes et al. 1980; Corbet et al. 1986) detected a shell-type profile of the emission line, that is a double-peaked profile in which the central absorption extends below the stellar continuum flux. According to the seminal model by Struve (1931, yet largely accepted; see Rivinius et al. 2013, for a more recent review), shell-type profiles imply an inclination angle of $i \sim 90°$ (i.e. an edge-on system). During our campaign we did not observe shell-type emission lines (see Fig. 2). Therefore, based on a qualitative comparison with Fig. 1 of Rivinius et al. (2013), the profiles detected in this work support a large ($60° \lesssim i \lesssim 80°$) inclination angle, yet not an edge-on view. Later, more physical models (Hummel 1994; Hanuschik 1996; Hummel & Hanuschik 1997) also support a large inclination angle. However, we should note here that line profile shapes do not always give unambiguous information about the disk inclination angle (Silaj et al. 2010; Quirrenbach et al. 1997). In any case, transient shell lines do not demand a tilt of the disk plane. For example, shell profiles need a geometrically thick medium to form. Therefore, the Hα line profiles observed in the present work may simply be due to a decrease of the disk density, with respect to previous conditions. Assuming typical values of the mass and radius of a B2 type star as $M_\star = 9.9\,M_\odot$, $R_\star = 5.4\,R_\odot$ (Townsend et al. 2004; Pasinetti-Fracassini et al. 2000; Sugizaki et al. 2015), the critical velocity of rotation is

$$V_{\text{break}} = \sqrt{\frac{GM_\star}{R_\star}} \approx 475\,\text{km s}^{-1}. \quad (4)$$

With an inclination angle $i = 90°$ and $V \sin i = 330\,\text{km s}^{-1}$, the resulting critical fraction is $w = V/V_{\text{break}} \approx 0.69$. On the other hand, assuming $w = 0.8$ and $V \sin i = 330\,\text{km s}^{-1}$, the resulting inclination angle is $i \sim 60°$, which is still consistent with the inclination inferred by the Hα line profile. We therefore conclude that, at least during our observations, a more conservative range for the inclination angle of V850 Cen is $60° \lesssim i \lesssim 90°$ and that V850 Cen is likely rotating at $0.69 \lesssim w \lesssim 0.80$.

3.2. The Hα line evolution

Table 2 summarizes the results of the spectral analysis, showing the evolution of Hα spectral parameters during the observational campaign. The evolution of the Hα emission line profile is also shown in Fig. 2, while a comparison of the Hα spectral parameters with the X-ray flux is shown in Fig. 3. From the latter plot, it is clear that the EW and the V/R ratio show a significant increase from the observation in 2014 to those in 2015. The EW doubled on a timescale of one year, while the V/R ratio increased by a factor of 4 in the same period. Despite the large variation in the V/R ratio, the dominant profile is always $V < R$. The

V/R variability is an important tracer of the disk activity. Indeed, while the strength of the Hα line (i.e., the EW) helps to trace size and density of the circumstellar disk (see Sect. 3.3), its morphology gives information about the degree of symmetry in the disk density, and in particular to possible global one-armed density oscillations (Oktariani & Okazaki 2009, and references therein). Our observations show that the disk density is asymmetrically distributed, likely due to a global density perturbation, and that the perturbation is still present at the smallest measured EW (i.e., at the smallest disk radius), although at a much lower degree. However, when the disk grows, the perturbation can develop further and the V/R ratio becomes higher. The relative intensity between the V and R peaks of Be stars in BeXRBs is found to cyclically vary (i.e. from $V < R$ to $V > R$, and vice versa) with a typical period of about 5 yr (Negueruela & Okazaki 2001; Reig et al. 2016). The very low value of the V/R ratio observed in 2014 possibly indicates that before our observation the V/R ratio was even lower, with a $V \approx R$ period, preceded by a $V > R$ phase.

The evolution of Hα spectral parameters seems also to reflect the evolution of X-ray production from the NS, as shown in Fig. 1. The minimum observed value of EW is obtained during the AAT observation on April 2014. Around that period, the X-ray source remained on a quiescent level during repeated periastron passages. One year later the EW increased significantly while, at the same time, the X-ray source was showing moderate activity (Nakajima et al. 2015). Therefore, higher X-ray fluxes are produced when the Hα line is stronger, that is, when the size of the Hα-emitting region (the circumstellar disk) is larger, thanks to the fact that larger disks get closer to the NS. Immediately before and after our SALT observations in 2015, the source shows moderate X-ray outbursts at the periastron passages (Nakajima et al. 2015), but the following outbursts are missing, showing minor and only sporadic periodical activity. This likely indicates that during our observations the circumstellar disk evolved from 2014 to 2015 in such a way that the transfer of a moderate amount of matter to the accreting NS was favored, but the disk conditions subsequently changed leading to the opposite trend. At the time of writing, the source has still not resumed its typical outburst X-ray intensity. This may be due to major disruption of the circumstellar disk, or perhaps to its distortion, thus preventing efficient accretion onto the NS. More quantitative considerations about the disk changes are discussed in the following sections.

3.3. Circumstellar Be disk size

The peak separation ΔV is an important parameter that helps to trace the circumstellar disk conditions: ΔV is related to the disk size and to the inclination angle i (see Eq. (2b)). A small peak separation results from a combination of a large circumstellar disk and a small inclination angle such that the disk is seen by the observer as almost uncovered by the central star (i.e., a face-on system). Conversely, a large peak separation results from a combination of a smaller disk and a large inclination angle such that the disk is heavily obscured by the central star (i.e., an edge-on system). For rotationally dominated line profiles, the peak separation ΔV of Hα emission lines can be used to estimate the size of the Hα-emitting region $R_{\rm d}$, that is, the circumstellar disk size (Huang 1972):

$$R_{\rm d} = \left(\frac{2V \sin i}{\Delta V}\right)^{j} \epsilon R_{\star} \tag{8}$$

where $j = 2$ for Keplerian rotation, $R_{\star}$ is the central star radius, and ϵ is a dimensionless parameter that takes into account several effects that would overestimate the disk radius, $\epsilon = 0.9 \pm 0.1$ (Zamanov et al. 2013). We note here that other works report the equation for $R_{\rm d}$ in another form (see e.g., Coe et al. 2006). However, Eq. (8) has two main advantages. First, it takes into account the (usually incorrect) assumption that the star is critically rotating and, second, it uses the $V \sin i$ quantity, which is obtained directly by observations. To calculate the disk radius, a stellar radius of $R_{\star} = 5.4\,R_{\odot}$ has been assumed (see Sect. 3.1), while $V \sin i$ has been derived by Eq. (2b). Figure 4 (middle panel) shows the disk radius $R_{\rm d}$ as a function of the EW(Hα) (absolute value). A positive correlation between the two parameters is found, in agreement with the expectation that the EW(Hα) reflects the size of the circumstellar disk (Quirrenbach et al. 1997; Grundstrom & Gies 2006).

Figure 4 (bottom panel) shows the peak separation ΔV as a function of the EW(Hα) (absolute value). A clear anti-correlation is present between the two parameters, indicating that as the disk radius (i.e., the EW) grows, the peak separation decreases. For strong EWs, the anti-correlation can be extrapolated down to a point where the two peaks merge ($\Delta V = 0$), and a single peaked Hα line emerges. For a number of BeXRBs, this occurs when the EW(Hα) becomes stronger than $\sim$−15 Å (Reig et al. 2016). However, our observations show that ΔV is still large at large disk radii ($|EW| > 15$ Å). This may be due to the large inclination angle i, which causes the disk to be seen almost edge-on. Indeed, if $i \sim 90°$, then it is difficult for the disk to emerge out of the optical companion obscuration, even at large radii. Also, results by Silaj et al. (2010) indicate that broadened double-peaked Hα profiles (thus large ΔV values) are expected at large inclination angles (see Fig. 5 in their work). On the other hand, as Reig et al. (2016) point out, the EW limit value is expected to depend on the spectral resolution, which, in their case, is generally much lower than ours (their spectra have typically $R < 2500$).

To better understand the accretion dynamics, it is also interesting to compare the circumstellar disk size with the NS distance from V850 Cen. Assuming $R_{\star} = 5.4\,R_{\odot}$, with $V \sin i$ and ΔV as observed with AAT (294 and 252 km s^{-1}, respectively, see Table 2), a disk radius of $R_{\rm d} \sim 2.2 \times 10^{10}$ m $\sim 5.9\,R_{\star}$ is obtained. On the other hand, assuming an orbital eccentricity of $e \sim 0.5$ and a semi-major axis of $a_x \sim 500$ lt-s (for an inclination angle $i = 90°$, Sugizaki et al. 2015), the obtained periastron distance is $a_{\rm peri} = a(1 - e) \sim 7.5 \times 10^{10}$ m $\sim 19\,R_{\star}$. Therefore, when the NS star approaches the periastron around the time of our AAT observation, the circumstellar matter is still within the Roche-lobe of V850 Cen ($R_{\rm RL} \sim 9\,R_{\star}$, calculated using the approximation by Eggleton 1983), and the transfer of matter onto the NS is completely inhibited. Indeed, the periodical X-ray outbursts around that period are missing (see Fig. 1). However, according to our SALT observations in 2015, during that epoch the disk radius grew up to $R_{\rm d} \sim 9$−$11\,R_{\star}$ and this was enough to allow the transfer of matter onto the NS, as reflected by the (weak) X-ray intensity of periodical outbursts during 2015. This is in agreement with the X-ray activity evolution observed at the two different epochs (see Fig. 1).

3.4. Inefficient tidal truncation

For closer binary orbits, the gravitational influence of the NS onto the circumstellar disk leads to resonances between the disk and the NS orbital period (Okazaki & Negueruela 2001;

Table 3. Spectral parameters of the Hβ emission line and derived disk parameters.

MJD	*EW* [Å]	*FWHM* [Å] (km s^{-1})	ΔV [km s^{-1}]	V/R	$R_{\rm disk}$ [$R_\star$]
56763	-5.6 ± 0.1	3.8 ± 0.1 (235 ± 3)	180 ± 2	0.35 ± 0.01	3.2 ± 0.6

Haigh et al. 2004; Coe et al. 2006). Such resonances tend to truncate the disk at specific radii, which can be calculated as (see also Grundstrom et al. 2007):

$$R_n^{3/2} = \frac{(GM_\star)^{1/2}}{2\pi n} P_{\rm orb} \quad (9)$$

where G is the gravitational constant, $M_\star$ is the central star mass, $P_{\rm orb}$ is the orbital period, and n is the integer number of disk rotational periods per orbital period. However, Okazaki & Negueruela (2001) proposed that in high-eccentricity binary systems, such as GX 304-1, disk truncation due to resonant effects is not efficient, and that the circumstellar disk radius is only limited by the closest approach of the NS to the companion, that is, by the periastron distance. Assuming $P_{\rm orb} = 132.189$ d and $M_\star = 9.9\,M_\odot$ (Sugizaki et al. 2015), the maximum observed disk radius ($R_{\rm d} \sim 11\,R_\star$, see Sect. 3.3) should be truncated by the 8:1 resonance, which implies an unusually high value of n for BeXRBs (see Monageng et al. 2017, and references therein), and possibly indicates that the disk size of V850 Cen as observed in the present work did not reach its largest possible radial extension. This possibility is further explored in the following.

We observe the strongest EW(Hα) during our SALT campaign at MJD 57 086, that is -39 Å. Among BeXRBs, the maximum observed EW is found to correlate with the orbital period of the binary system $P_{\rm orb}$ (Reig et al. 1997; Antoniou et al. 2009; Coe & Kirk 2015) and with the periastron distance (Reig et al. 2016). According to those authors, an orbital period of ~132 d (or, similarly, a periastron distance of $19\,R_\star$) would imply an EW of the Hα emission line between -30 and -40 Å. This is consistent with our observations, suggesting that the circumstellar disk of V850 Cen was approaching its maximum size around the time of observations with SALT. However, our optical observations do not cover a typical X-ray outburst; the X-ray flux of periodical outbursts observed immediately before and after our SALT campaign is about half of the GX 304-1 standard ones (see Fig. 1). The lower X-ray flux is due to the lower mass accreted by the NS, which in turn reflects the lack of disk material in the vicinity of the compact object. Within this interpretation it is therefore possible that the maximum EW value observed in the present work does not represent the actual maximum size reachable by the circumstellar disk but rather a lower limit on the maximum size, thus allowing GX 304-1 to deviate from the above-mentioned correlations. Since those correlations have been interpreted as evidence of disk truncation, the possibility of GX 304-1 deviating from them is still consistent with the model of inefficient tidal truncation in GX 304-1 proposed by Okazaki & Negueruela (2001).

Finally, we note that typical circumstellar disk radii in BeXRBs have $\lesssim 6\,R_\star$ (Reig et al. 2016). This value is smaller than that of circumstellar disk radii in isolated Be stars ($\gtrsim 14\,R_\star$). Also, the resulting upper limit value is independent from the donor star size. The above considerations suggest that the maximum extent of the disk is a characteristic quantity of binary systems in which tidal truncation is at work. On the other hand, V850 Cen develops a disk at least as large as $\sim 11\,R_\star$. Again, this result can be interpreted as a possible hint for inefficient tidal truncation in GX 304-1.

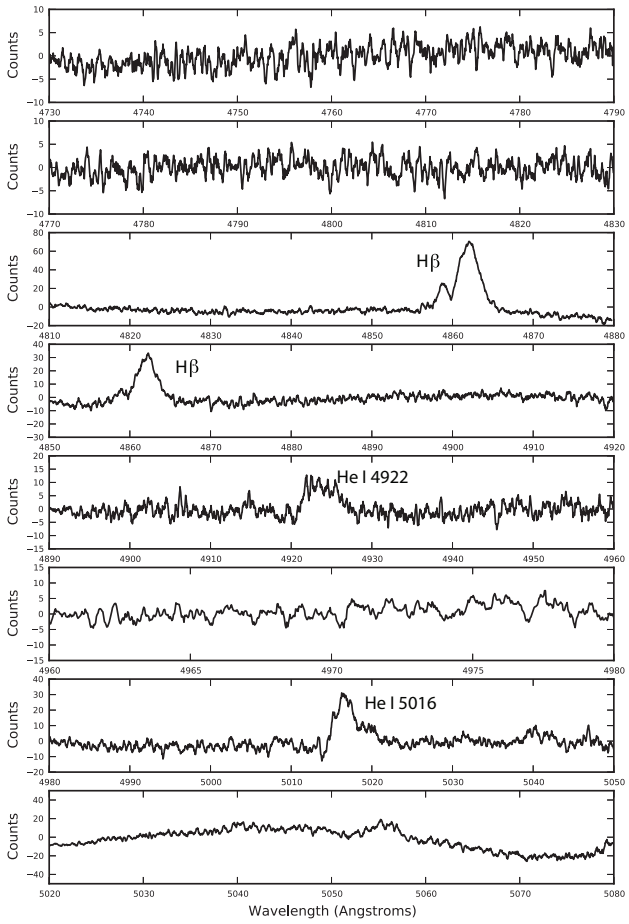

Fig. 5. Selection of AAT/UCLES orders at bluer wavelengths. Highlighted are the prominent Hβ line and He I 4922, 5016 features.

3.5. The Hβ emission line

Data from the AAT observation in 2014 allowed us to measure the spectral parameters of the Hβ emission line. For this, we applied the same procedure used for the measurement of Hα line parameters (see Sect. 3.1). The results are summarized in Table 3, while a selection of bluer AAT orders including the Hβ emission line is shown in Fig. 5. The very presence of a Hβ emission line indicates that the disk is already dense, even at its smallest measured radius. The Hβ emitting disk radius has been calculated according to Eq. (8), adopting a value of $j = 1$ (Mennickent & Vogt 1991) and results of about $3.2\,R_\star$. This is in agreement with observations of Hβ emitting disks in other Be stars (Mennickent 1991; Zamanov et al. 2016). However, we note that, contrary to other Be star observations (Hanuschik et al. 1988; Zamanov et al. 2016), the Hβ peak separation (and the

overall line shape) appears smaller than the Hα. In the case of Hanuschik et al. (1988) the spectral resolution of the employed instrument is of the order of $R \sim 10^5$, and this can be a possible reason for the observed discrepancy. Moreover, as in the case for the Hα line, the Hβ also shows a $V < R$ line profile, indicating that the asymmetry in the disk density extends down to smaller radii.

Finally, the EWs of Hα and Hβ lines can be compared to constrain the luminosity class of optical companions in high-mass X-ray binaries (Reig et al. 1996; Fabregat et al. 1996). Our results suggest a luminosity class III–V, which is consistent with the stellar classification proposed by Parkes et al. (1980).

4. Conclusions

We have analyzed optical spectra of V850 Cen, the donor star of the BeXRB GX 304-1. Data were taken with the AAT/UCLES and SALT/HRS, spanning over one year and distributed along the orbital period of the binary system. Our study has focused on the Balmer emission lines, and the characterization of the circumstellar disk, in order to gain insight into the connection between the stellar wind structure of V850 Cen and the X-ray activity of GX 304-1. Our main results are summarized as follows:

- During all our observations, the Hα line is always present in emission. Its profile is always double-peaked, although it shows strong variation on a time scale of ~1 yr.
- Our observations support a large inclination angle, that is, $i \gtrsim 60°$, possibly an edge-on system.
- The Hα-emitting circumstellar disk has a size that ranges from $\sim 5.9\,R_\star$ in 2014 to $\sim 11\,R_\star$ one year later. With a Roche-lobe at the periastron of $R_{\rm RL} \sim 9\,R_\star$, the X-ray intermittent activity of GX 304-1 is a direct consequence of the circumstellar disk evolution.
- Several pieces of evidence point to the possibility of inefficient truncation of the circumstellar disk by the orbiting NS, as expected from theoretical arguments for this source's binary configuration. However, no firm conclusion can be drawn from our data on this particular subject.
- Detection of the Hβ emission line and its comparison to the Hα line allow us to derive a circumstellar disk size of the Hβ emitting region that is about half of the Hα-emitting disk and to constrain the luminosity class of the source as III–V, consistent with the previously proposed class.

Acknowledgements. We gratefully acknowledge the anonymous referee for numerous comments that greatly improved the manuscript. Some of the data used in this paper were acquired through the Australian Astronomical Observatory, via program UC205, while other observations were obtained with the Southern African Large Telescope (SALT/HRS). This work is supported by the Bundesministerium für Wirtschaft und Technologie through the Deutsches Zentrum für Luft- und Raumfahrt e.V. (DLR) under the grants FKZ 50 OR 1204. L.D. acknowledges the grant FKZ 50 OG 1602. W.K. acknowledges the grant DFG Ko 857/32-2.

References

Antoniou, V., Hatzidimitriou, D., Zezas, A., & Reig, P. 2009, ApJ, 707, 1080
Coe, M. J., & Kirk, J. 2015, MNRAS, 452, 969
Coe, M. J., Reig, P., McBride, V. A., Galache, J. L., & Fabregat, J. 2006, MNRAS, 368, 447
Corbet, R. H. D., Smale, A. P., Menzies, J. W., et al. 1986, MNRAS, 221, 961
Devasia, J., James, M., Paul, B., & Indulekha, K. 2011, MNRAS, 417, 348
Eggleton, P. P. 1983, ApJ, 268, 368
Fabregat, J., Capilla, G., & Reig, P. 1996, Mem. Soc. Astron. It., 67, 333
Grundstrom, E. D., & Gies, D. R. 2006, ApJ, 651, L53
Grundstrom, E. D., Boyajian, T. S., Finch, C., et al. 2007, ApJ, 660, 1398
Haefner, R. 1988, Information Bulletin on Variable Stars, 3260, 1
Haigh, N. J., Coe, M. J., & Fabregat, J. 2004, MNRAS, 350, 1457
Hanuschik, R. W. 1989, Ap&SS, 161, 61
Hanuschik, R. W. 1996, A&A, 308, 170
Hanuschik, R. W., Kozok, J. R., & Kaiser, D. 1988, A&A, 189, 147
Hewish, A., Bell, S. J., Pilkington, J. D. H., Scott, P. F., & Collins, R. A. 1968, Nature, 217, 709
Horton, A., Tinney, C. G., Case, S., et al. 2012, in Ground-based and Airborne Instrumentation for Astronomy IV, Proc. SPIE, 8446, 84463A
Huang, S.-S. 1972, ApJ, 171, 549
Hummel, W. 1994, A&A, 289, 458
Hummel, W., & Hanuschik, R. W. 1997, A&A, 320, 852
Jaisawal, G. K., Naik, S., & Epili, P. 2016, MNRAS, 457, 2749
Kızıloğlu, U., Kızıloğlu, N., Baykal, A., Yerli, S. K., & Özbey, M. 2007, A&A, 470, 1023
Klochkov, D., Doroshenko, V., Santangelo, A., et al. 2012, A&A, 542, L28
Lewin, W. H. G., Clark, G. W., & Smith, W. B. 1968, Nature, 219, 1235
Malacaria, C., Klochkov, D., Santangelo, A., & Staubert, R. 2015, A&A, 581, A121
Manousakis, A., Beckmann, V., Bianchin, V., et al. 2008, ATel, 1613, 1
Martin, R. G., Nixon, C., Armitage, P. J., Lubow, S. H., & Price, D. J. 2014, ApJ, 790, L34
Mason, K. O., Murdin, P. G., Parkes, G. E., & Visvanathan, N. 1978, MNRAS, 184, 45P
McClintock, J. E., Nugent, J. J., Li, F. K., & Rappaport, S. A. 1977, ApJ, 216, L15
Mennickent, R. E. 1991, A&AS, 88, 1
Mennickent, R. E., & Vogt, N. 1991, A&A, 241, 159
Monageng, I. M., McBride, V. A., Coe, M. J., Steele, I. A., & Reig, P. 2017, MNRAS, 464, 572
Nakajima, M., Mihara, T., Ono, Y., et al. 2015, ATel, 7441
Negueruela, I., & Okazaki, A. T. 2001, A&A, 369, 108
Okazaki, A. T., & Negueruela, I. 2001, A&A, 377, 161
Okazaki, A. T., Hayasaki, K., & Moritani, Y. 2013, PASJ, 65, 41
Oktariani, F., & Okazaki, A. T. 2009, PASJ, 61, 57
Parkes, G. E., Murdin, P. G., & Mason, K. O. 1980, MNRAS, 190, 537
Pasinetti-Fracassini, L. E., Pastori, L., Covino, S., & Pozzi, A. 2000, VizieR Online Data Catalog: II/224
Pietsch, W., Oegelman, H., Kahabka, P., Collmar, W., & Gottwald, M. 1986, A&A, 163, 93
Porter, J. M. 1996, MNRAS, 280, L31
Porter, J. M. 1998, A&A, 336, 966
Porter, J. M., & Rivinius, T. 2003, PASP, 115, 1153
Priedhorsky, W. C., & Terrell, J. 1983, ApJ, 273, 709
Quirrenbach, A., Bjorkman, K. S., Bjorkman, J. E., et al. 1997, ApJ, 479, 477
Rajoelimanana, A. F., Charles, P. A., Meintjes, P. J., et al. 2017, MNRAS, 464, 4133
Reig, P., Chakrabarty, D., Coe, M. J., et al. 1996, A&A, 311, 879
Reig, P., Fabregat, J., & Coe, M. J. 1997, A&A, 322, 193
Reig, P., Negueruela, I., Fabregat, J., et al. 2004, A&A, 421, 673
Reig, P., Zezas, A., & Gkouvelis, L. 2010, A&A, 522, A107
Reig, P., Nersesian, A., Zezas, A., Gkouvelis, L., & Coe, M. J. 2016, A&A, 590, A122
Rivinius, T., Štefl, S., & Baade, D. 2006, A&A, 459, 137
Rivinius, T., Carciofi, A. C., & Martayan, C. 2013, A&ARv, 21, 69
Rothschild, R. E., Kühnel, M., Pottschmidt, K., et al. 2017, MNRAS, 466, 2752
Silaj, J., Jones, C. E., Tycner, C., Sigut, T. A. A., & Smith, A. D. 2010, ApJS, 187, 228
Steele, I. A., Negueruela, I., & Clark, J. S. 1999, A&AS, 137, 147
Struve, O. 1931, ApJ, 73, 94
Sugizaki, M., Yamamoto, T., Mihara, T., Nakajima, M., & Makishima, K. 2015, PASJ, 67, 73
Townsend, R. H. D., Owocki, S. P., & Howarth, I. D. 2004, MNRAS, 350, 189
Tyas, L. M. G. 2012, Ph.D. Thesis, Durham University
van Belle, G. 2008, Sample Size (John Wiley & Sons, Inc.), 27
Yamamoto, T., Sugizaki, M., Mihara, T., et al. 2011, PASJ, 63, S751
Zamanov, R. K., Reig, P., Martí, J., et al. 2001, A&A, 367, 884
Zamanov, R., Stoyanov, K., Martí, J., et al. 2013, A&A, 559, A87
Zamanov, R. K., Stoyanov, K. A., Martí, J., et al. 2016, A&A, 593, A97